Hindawi
Shock and Vibration
Volume 2019, Article ID 5792841, 7 pages
https://doi.org/10.1155/2019/5792841

Research Article

Dynamic Compression Damage Energy Consumption and Fractal Characteristics of Shale

Guoliang Yang,[1,2] Jingjiu Bi,[1] and Linian Ma[1]

[1]*School of Mechanics and Civil Engineering, China University of Mining and Technology, Beijing 100083, China*
[2]*State Key Laboratory of Explosion Science and Technology, Beijing, China*

Correspondence should be addressed to Jingjiu Bi; sqt1700602039@student.cumtb.edu.cn

Received 17 June 2019; Accepted 6 September 2019; Published 23 September 2019

Academic Editor: Roberto Palma

Studying the relationship between energy consumption and crushed size of shale under different loading conditions is the key to efficient shale cracking. The split Hopkinson pressure bar system was used to study the dynamic mechanical properties of shale under parallel- and vertical-bedding loading, and energy dissipation in the impact tests was calculated. Relationships between the average crushed size of shale fracture products and energy dissipation and between the fractal dimension and dissipated energy were studied using fractal theory. The experimental results showed that the dynamic compressive strength of shale under parallel- and vertical-bedding conditions had an obvious positive correlation with the strain rate. Dissipative energy of the shale samples under loading in both directions increased with the increase of strain rate. The increase of the strain rate enhanced crushing of the sample. The vertical-bedding shale samples had stronger ability to absorb energy and more internal crack propagation. Dissipative energies of the shale samples in the parallel- and vertical-bedding impact tests were positively related to the fractal dimension. The fractal dimension increased with the increase of dissipative energy during sample failure; with further increase in the dissipative energy, its effect on the change of fractal dimension gradually weakened.

1. Introduction

The core purpose of shale-gas mining technology is to carry out reservoir reconstruction of shale-gas reservoirs and to break the rock formation using techniques such as hydraulic fracturing. With the development of new fracturing technologies, such as through-liquid gunpowder high-energy gas fracturing and others, dynamic shale fracturing is expected to become an effective technology to increase production. It is therefore necessary to study the dynamic mechanical response of shale during dynamic fracturing [1].

The split Hopkinson pressure bar (SHPB) is an effective method for studying mechanical properties of rock under impact loading. Yue et al. [2] used a modified SHPB device to perform uniaxial impact compression experiments on granite samples from the Bukit Timah area of Singapore at different strain rates. The results showed that the dynamic resistance of granite increased with an increase of strain rate. The compressive strength increased simultaneously with an increase in the crushed size of the granite, and the size and number of fragments increased. Dan et al. [3] used an SHPB to carry out multiple-impact loading experiments on granite samples and obtained sets of waveform curves under high strain rates. They concluded that the peak stress, peak strain, and dissipative energy increased with the increase of strain rate.

Macroscopic fracture of rock is the final result of the continuous development, expansion, aggregation, and penetration of its internal defects. Progress from mesoscopic damage to macroscopic fracture is an energy-dissipation process and has fractal properties. From the perspective of energy, the deformation and failure of rock have been analyzed and the relationship between rock failure and energy change is established. Sujatha and Chandra Kishen [4] proposed that each stress-strain state of rock is linked to a corresponding energy state. From elastic deformation and microcrack evolution, for destruction, energy exchange with the outside world is always stored and the energy transmitted by the outside world is stored. This process also releases energy to the outside world in various forms to

maintain an energy balance. Xie et al. [5] analyzed energy dissipation and release during uniaxial compression failures of granite, limestone, and sandstone. Experimental research showed that energy played a fundamental role in the process of rock deformation and failure: the sudden release of energy caused instability of the rock.

Owing to the irregularity of fracture surfaces of rock, it is difficult to approximate its simulation using a flat surface [6]; rather, the application of fractal theory in rock fracture can truly describe the fracture shape [7]. Using a large number of experimental observations, macroscopic fracture of the material has self-similarity; the behavior of this self-similarity will inevitably lead to self-similarity of the fragmentation and energy dissipation after fracture [8–10]. Xie et al. [11], through a large number of experiments combined with fractal theory, found that the larger the fractal dimension, the higher the crushed size of the rock mass, the greater the amount of fragmentation, and the smaller the volume after fragmentation. The fractal dimension of the block distribution could quantitatively reflect the size of the crushed rock. Shi et al. [12] conducted impact compression tests on sericite-quartz schist and sandstone using an SHPB device, obtained the fractal dimension of the crushed rock size under impact load using fractal geometry theory, and studied the influence of impact velocity on the fractal dimension.

Under impact loading conditions, shale exhibits significant anisotropy. Studying the relationship between its energy consumption and crushed size under different loading conditions is the key to efficient shale cracking. In this work, impact compression tests on parallel- and vertical-bedding shale samples were carried out using an SHPB device to study the energy dissipation under impact loads at 0° and 90° to the bedding directions. The relationship between the loading rate and energy dissipation of the shale under dynamic impact was established. Fractal theory was used to calculate the average crushed size and fractal dimension. Fractal characteristics of the fractured block were analyzed. Relationships between the average crushed size and energy dissipation of the fracture product and between the fractal dimension and dissipation energy were obtained.

2. Materials and Methods

2.1. Sample Preparation and Test Device. The samples used in this work were taken from outcrop shale of the Longmaxi Formation in the Changning area of Sichuan Province, China. To avoid large dispersion of the test results due to sampling differences, the samples were taken from the same batch of rock. A 75 mm cylindrical sample was drilled in the parallel-bedding and vertical-bedding directions using a core drill, as shown in Figure 1. After being cut and polished, the samples were processed into 75 mm × 37.5 mm discs. Each disc had an error of 0.5 mm in length and an end-face flatness error of 0.02 mm.

Using a 75 mm diameter SHPB device for dynamic rock testing, different strain rates were achieved by changing the magnitude of the impact gas pressure. The impact gas pressure was selected from five settings: 0.62, 0.64, 0.66, 0.68, and 0.70 MPa. Each experiment was carried out in triplicate.

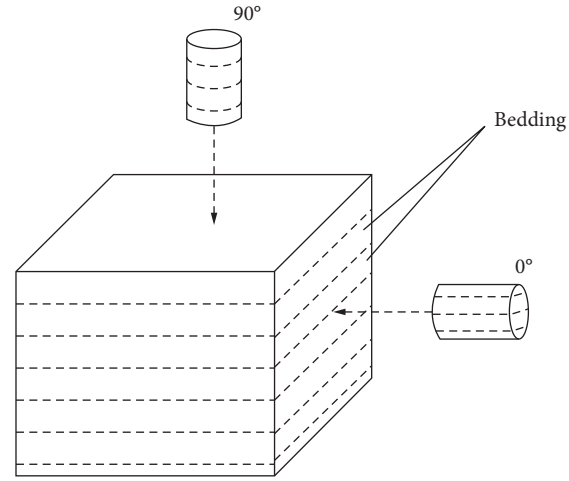

Figure 1: Schematic diagram of coring of the shale sample.

2.2. Principle of Energy Analysis of Split Hopkinson Pressure Bar System. The Hopkinson bar test system was used to dynamically impact the rock. From the start of loading to failure of the sample, the energies carried by the incident, reflected, and transmitted waves were W_I, W_R, and W_T, respectively. The calculations are as follows [13, 14]:

$$W_I = A_0 C_0 E_0 \int_0^\tau \varepsilon_I^2 dt,$$
$$W_R = A_0 C_0 E_0 \int_0^\tau \varepsilon_R^2 dt, \quad (1)$$
$$W_T = A_0 C_0 E_0 \int_0^\tau \varepsilon_T^2 dt,$$

where A_0, C_0, and E_0, respectively, indicate the cross-sectional area of the strut, the stress-wave velocity, and the elastic modulus.

The two end surfaces of the sample were coated with petroleum jelly as a lubricant, so energy dissipation caused by friction between the sample and the contact end surfaces of the incident and transmission bars during the loading process did not need to be considered in the energy analysis.

Energy dissipated in the test sample was calculated using the following formula [4]:

$$W_L = W_I - W_R - W_T. \quad (2)$$

W_L can be divided into three parts: (i) fracture dissipation energy W_F, which is mainly used for crack damage formation and fracture surface formation; (ii) kinetic energy W_K, associated with the ejection of sample fragments; and (iii) other forms of energy dissipation W_O, such as sound and radiant energy. When the loading rate is not particularly high, W_O is very small to negligible and kinetic energy of the sample fragments accounts for about 5% of W_L. This test analyzes the dissipative energy of the sample by ignoring the kinetic energy of the sample fragments.

3. Results and Analysis

3.1. Dynamic Compressive Strength of Shale Samples under Different Loading Conditions. Typical stress-strain curves obtained in these tests are shown in Figures 2 and 3. The curves can be divided into four stages: initial deformation, linear elastic deformation, nonlinear deformation, and rock failure unloading.

Comparison of Figures 2 and 3 shows that when the strain rates were similar, the peak stress of the parallel-bedding-loaded shale sample was larger than that of the vertical-bedding-loaded sample; the peak strain of the parallel-bedding-loaded shale was smaller than that of vertical-bedding shale. The average slope of the elastic section of the curves was taken as the elastic modulus of the shale: the elastic modulus of the parallel-bedding-loaded shale was larger than that of the vertical-bedding-loaded sample.

As the rock is loaded under different schemes, the type of rock damage will change. When subjected to dynamic loads, a rock will converge a large amount of energy in a very short time, which will cause cracks within the rock to crack in different directions under high-speed impact. The failure mechanism of rock under high-speed impact is close to the failure mode in actual engineering. Figure 4 shows typical failure modes of shale samples under parallel- and vertical-bedding loading under an impact gas pressure of 0.70 MPa.

The compressive strength and strain rate of the test sample were obtained by data processing. The curves after fitting the data are shown in Figure 5, where P indicates parallel bedding and C indicates vertical bedding. The dynamic compressive strength had significant strain-rate correlation and increased with the increase of the strain rate, which was approximately linear. Comparing the linear relationships in the two cases, it was found the slope in the parallel-bedding case was larger than that in the vertical-bedding case, indicating that the dynamic compressive strength of the former was more sensitive to the strain rate. The dynamic compressive strength of parallel-bedding samples was greater than that of vertical-bedding samples.

3.2. Dissipation Energy of Shale Samples under Different Loading Conditions. According to the energy calculation formula obtained from the Hopkinson bar experimental principle and the stress-wave data obtained from the tests, the incident, reflected, and transmission energies and the energy consumed by the sample rupture during the test were calculated and the data were processed. Statistical results for different energies were obtained and the data were fitted, as shown in Figures 6 and 7.

Figure 6 shows that the dissipated energy of shale increased with the increase of incident energy under the two bedding conditions, according to a linear relationship. This indicated that the proportionality between the dissipative energy of shale rupture and the incident energy was relatively constant.

Figure 7 shows that dissipative energy of shale samples increased with the increase of the strain rate for both loading directions. This is because, as the strain rate increased, a greater number of new cracks were generated in the sample and more dissipative energy was absorbed. The increase of the strain rate enhanced breaking of the sample.

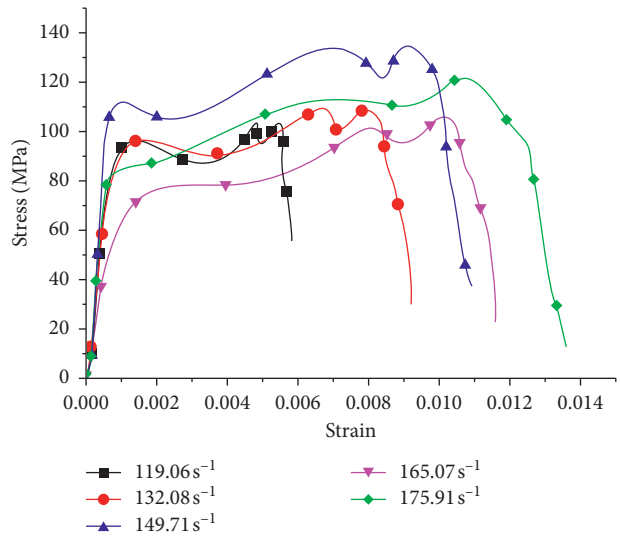

Figure 2: Typical stress-strain curves of parallel-bedding shale samples at different strain rates.

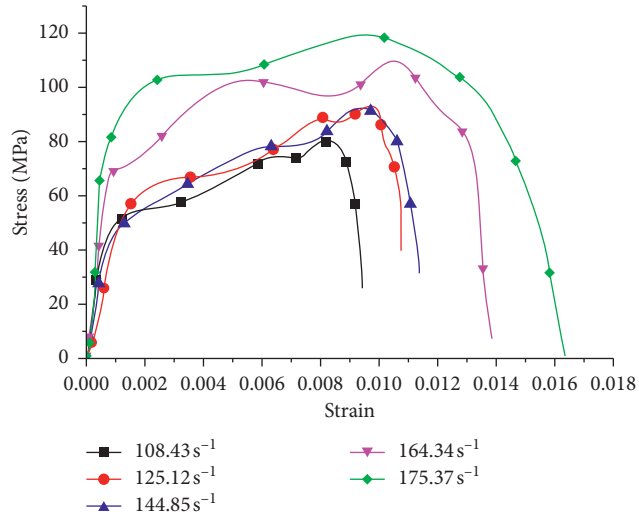

Figure 3: Typical stress-strain curves of vertical-bedding shale samples at different strain rates.

Combining the data in Figures 6 and 7, for the case of the same incident energy, the energy absorbed by the vertical-bedding shale sample was greater than that absorbed by the parallel-bedding sample, reflecting the difference in the abilities of these two beddings to absorb energy. This is mainly related to the distribution and arrangement of sedimentary bedding, stratified flake minerals, and organic matter in the shale. Vertically stratified shale samples had a greater ability to absorb energy, and the number of internal cracks propagated and the degree of fragmentation were greater.

3.3. Shale Fracture Fractal Study. The crushed shale products of the dynamic impact tests were collected and combined in

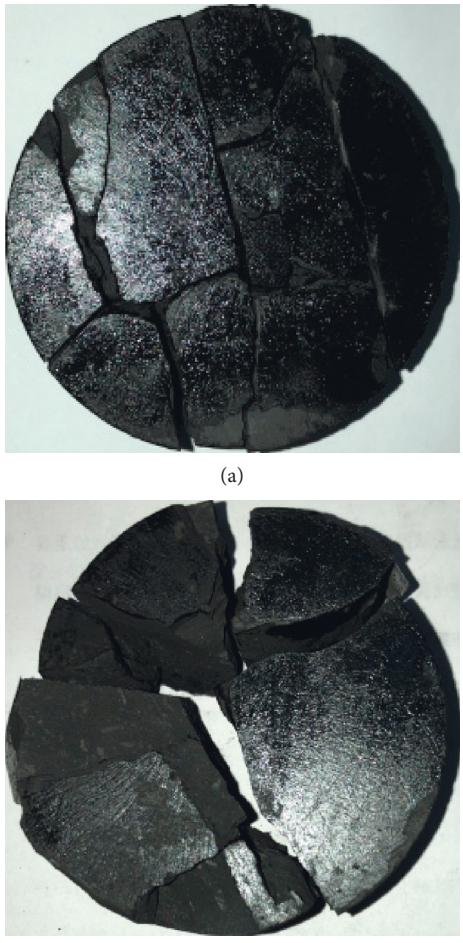

(a)

(b)

Figure 4: Typical shale rupture morphology: (a) parallel bedding; (b) vertical bedding.

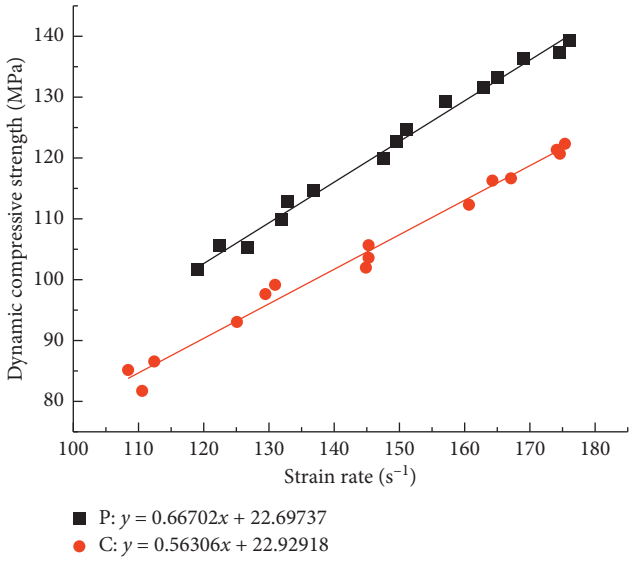

Figure 5: Dynamic compressive strength as a function of strain rate for parallel- (P-) bedding and vertical- (C-) bedding samples.

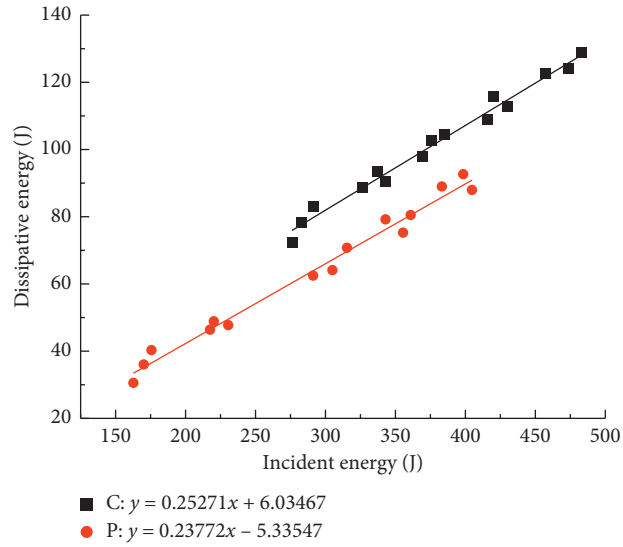

Figure 6: Relationship between dissipative and incident energies when parallel (P) and vertical (C) beddings were loaded.

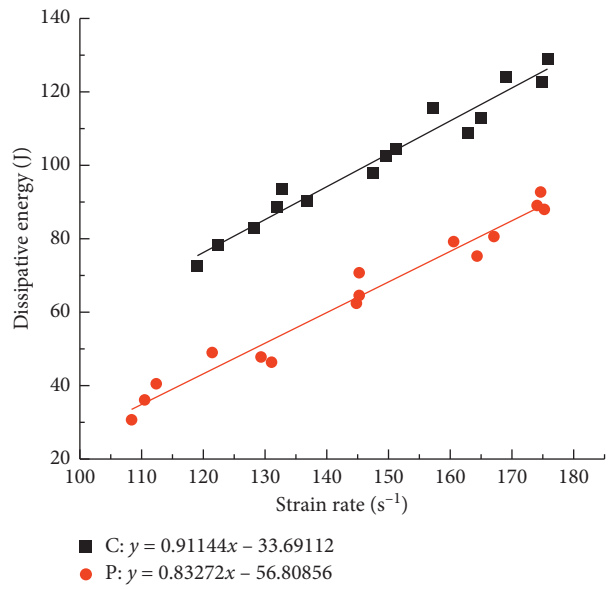

Figure 7: Relationship between dissipative energy and strain rate for parallel- (P-) bedding and vertical- (C-) bedding samples.

size fractions according to standard laboratory sieve sizes of 2.36, 4.75, 9.5, 16, 19, 26.5, 31.5, 37.5, and 53 mm. A high-sensitivity electronic balance was used to weigh the mass accumulated on each sieve after screening, and the data were recorded for block size analysis.

To more intuitively and accurately represent the particle size distribution of the shale sample after fracture, we introduced the physical quantity of the average crushed size, calculated as follows [5]:

$$\overline{d} = \frac{\sum(r_i d_i)}{\sum r_i}, \tag{3}$$

where $\overline{d}$ represents the average particle size of the shale sample after impact crushing, d_i represents the average particle size of the crushed block accumulated on the sieve after the screening test, and r_i represents the d_i size corresponding to the mass of the broken block. Assuming that the maximum particle size of the fractured block was 75 mm in diameter and the minimum value was 0 mm, the values of d_i were 64, 45.25, 34.5, 29, 22.75, 17.5, 12.75, 7.125, 3.555, and 1.18 mm. The vibration sieve machine and the examples of the shale sample after screening are shown in Figures 8 and 9.

From the perspective of fractal analysis, the fracture shape of the block after rock rupture is similar to the shape of the enlarged fracture; that is, various geometric shapes after rock rupture have self-similarity. The fractal dimension of the broken block of a shale sample can be obtained from the following formula [15]:

$$\lg y_i = \lg\left(\frac{M_i}{M}\right) = (3 - D)\lg\left(\frac{x_i}{x_q}\right), \quad (4)$$

where x_i is the line dimension of the i-th fragment; y_i is the volume of the block with a broken block size not greater than x_i, the mass sum of which is in proportion to the total volume (total mass); M_i is the mass of a block, the broken block size of which is not greater than x_i; M is the total mass; and x_q is the source block line size D for fractal dimensions. On obtaining the fitted line of $\lg(M_i/M) - \lg(x_i/x_q)$, the slope of the line is $(3 - D)$.

The posttest data were collated, and the average crushed size and strain rate under parallel and vertical beddings of shale were, respectively, fitted to obtain the relationship curves shown in Figure 10.

Figure 10 shows that the shale samples had different fracture size distributions after failure at different strain rates obtained under different atmospheric pressure impacts. After dynamic impact compression of the parallel and vertical beddings, the average crushed size of the fragments rapidly decreased with the increase of the strain rate, but as the strain rate continued to increase, the slope of the curve gradually became smaller, indicating that the influence of the strain rate on the average crushed size was gradually reduced. The test data were further sorted, and the incident energy, dissipated energy, and average crushed size of the parallel- and vertical-bedding samples were, respectively, matched. The fitting relationship curves are shown in Figures 11 and 12, respectively.

The average crushed size after dynamic impact compression was reduced with an increase of the dissipation energy, but as the dissipation energy increased gradually, the slope of the fitted curve began to decrease and the effect on crushed size was reduced. The relationship between the macroscopic fracture of the shale sample and the energy absorbed (dissipative energy) is relatively tight. As the incident energy increased, the dissipated energy absorbed by the sample increased and there was an increase in the number of cracks generated. The larger the number of block products after crushing, the smaller their size after the sample was broken.

The test data were further sorted, and the dissipative energy for the parallel- and vertical-bedding samples was

Figure 8: Vibration sieve machine.

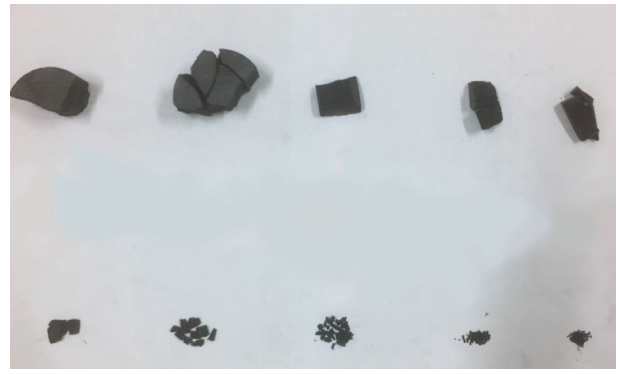

Figure 9: Examples of the shale sample after screening.

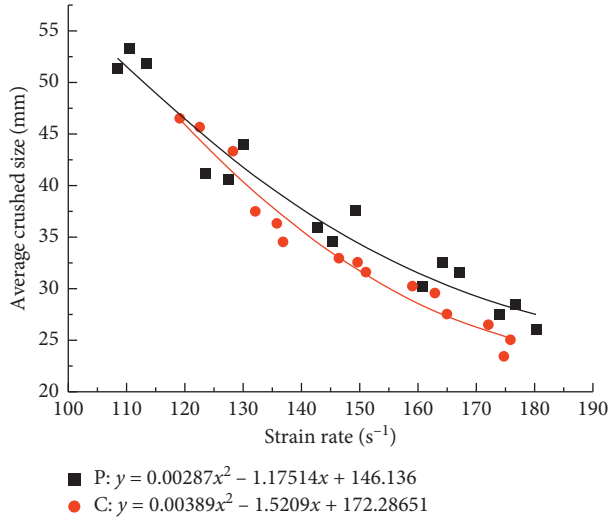

Figure 10: Relationship between the average crushed size and the strain rate of shale under dynamic compression loading of parallel (P) and vertical (C) beddings.

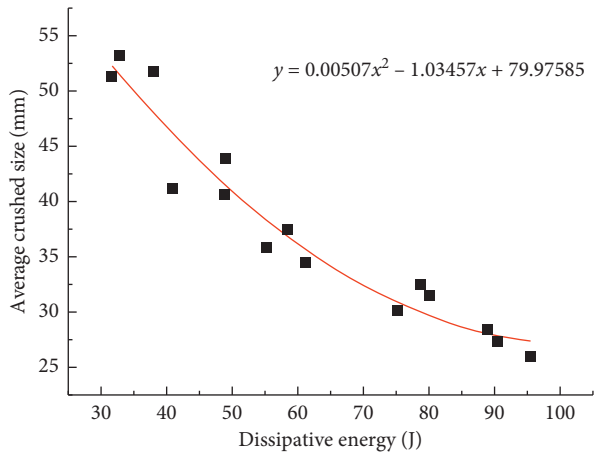

Figure 11: Relationship between the average crushed size and the dissipative energy of parallel-bedding shale under dynamic compression.

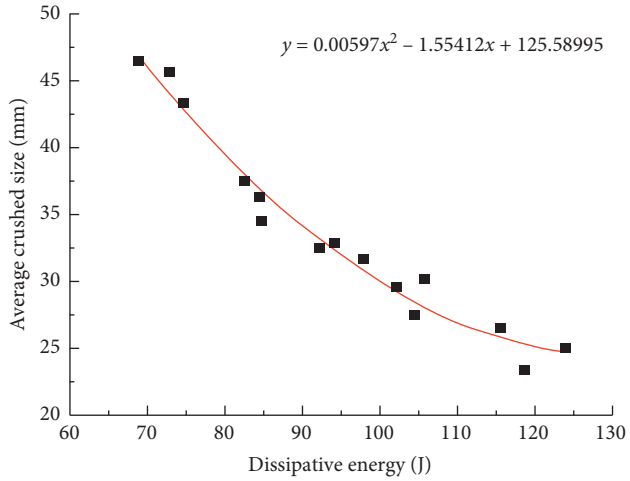

Figure 12: Relationship between the average crushed size and the dissipative energy of vertical-bedding shale under dynamic compression.

matched with the fractal dimension of the broken block. The curves of the fitted relationships are shown in Figure 13.

Analysis of Figure 13 shows that the rupture dissipation energy of shale samples in both bedding directions was positively related to the fractal dimension of the rock mass after rupture. The fractal dimension increased with the increase of dissipative energy during destruction of the sample in accordance with polynomial functions. Combining this information with fracture of the sample, it can be seen that the more the energy consumed during the rupture process, the larger the fractal dimension. The smaller the crushed size, the greater the number of resulting blocks after rupture. Figure 13 shows that as the dissipative energy gradually increased, the slopes of the fitted curves became smaller, indicating that the rate of increase of the fractal dimension slowed down, eventually reaching a limiting value. The effect of increasing dissipative energy on the change of the fractal dimension gradually weakened. The

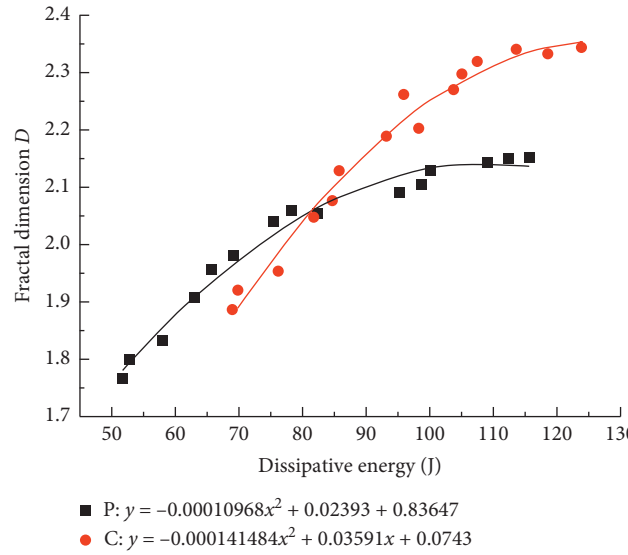

Figure 13: Relationships between the fractal dimension of parallel- and vertical-bedding samples and rupture dissipation energy.

slopes of the fitted relationships between the fractal dimension and dissipative energy of the vertical-bedding shale were large in Figure 13, indicating that the fractal dimension of the vertical-bedding shale was more sensitive to the variation of dissipation energy. The change in crushed size was more strongly affected by the increase in dissipative energy.

4. Conclusions

The dynamic mechanical properties of shale were experimentally studied. Parallel-stratification and vertical-bedding shale samples were subjected to dynamic impact compression loading tests using an SHPB test system. The dynamic compressive strength, stress-strain relationship, and failure mode of the two shale types under impact loading were analyzed, and the energy consumption and fractal characteristics were determined. The following conclusions were drawn:

(1) Dynamic compressive strength of shale under parallel- and vertical-bedding conditions had an obvious correlation with the strain rate and increased with the increase of the strain rate in an approximately linear manner. When the strain rates were similar, the peak stress of the parallel-bedding shale sample was larger than that of the vertical-bedding sample; the peak strain of the parallel-bedding-loaded shale sample was smaller than that of the vertical-bedding sample.

(2) Analysis of the energy consumption of parallel- and vertical-bedding shale under a dynamic impact load showed that, with the increase of the strain rate, the dissipative energy absorbed by the sample increased, indicating that the strain rate increased. This effect enhanced crushing of the shale samples. The energy absorbed by the vertical-bedding shale sample was

greater than that absorbed by the parallel-bedding sample, reflecting their difference in energy absorption capacity. The stronger the ability of the shale to absorb energy, the greater the number of internal cracks propagated.

(3) By analyzing the particle size distribution of the shale sample after failure and introducing fractal theory, it was shown that the average crushed size obtained from dynamic impact compression damage increased with the dissipation energy for both the parallel-bedding and vertical-bedding shale samples. The variation in the average crushed size following dynamic compression with the increase of dissipative energy was more obvious for the vertical-bedding shale, and the crushed size was smaller. Dissipative energy had a positive correlation with the fractal dimension of the rock mass. The fractal dimension increased as the dissipative energy increased during failure of the sample. With the increase of dissipative energy, the influence of the variation of dissipative energy on the change of the fractal dimension gradually weakened. Compared with parallel-bedding shale, the fractal dimension and crushed size of vertical-bedding shale were more affected by the variation of dissipation energy.

Data Availability

The data used to support the findings of this study are available from the corresponding author upon request.

Conflicts of Interest

The authors declare that there are no conflicts of interest regarding the publication of this paper.

Acknowledgments

This paper was supported by the opening project of State Key Laboratory of Explosion Science and Technology, Beijing Institute of Technology (no. KFJJ19-10M).

References

[1] C. Junbin, *Research on Key Technology for Shale Gas Reservoir Liquid Gunpowder High Energy Gas Fracturing Stimulation*, Science Press, Beijing, China, 2017.

[2] Y. Yue, G. Ma, J. Zhao, and C. Hu, "Dynamic fracture analysis of granite under uniaxial impact compression loading," *Chinese Journal of Geotechnical Engineering*, no. 3, pp. 385–390, 2007.

[3] L. Dan, W. Yan, and Y. Wang, "Analysis of strain rate effect of granite based on SHPB," *Journal of Hebei North University (Natural Science Edition)*, vol. 32, no. 9, pp. 29–35, 2016.

[4] V. Sujatha and J. M. Chandra Kishen, "Energy release rate due to friction at bi-material interface in dams," *Journal of Engineering Mechanics, ASCE*, vol. 129, no. 7, pp. 793–800, 2003.

[5] H. Xie, R. Peng, Y. Yang et al., "Preliminary study on energy analysis of rock failure," *Chinese Journal of Rock Mechanics and Engineering*, vol. 24, no. 15, pp. 2603–2608, 2005.

[6] P. J. Perie, "Determination of fracture mechanism by microscopic observation of crack," *International Journal of Rock Mechanics and Mining Sciences & Geomechanics Abstracts*, vol. 28, no. 1, pp. 83-84, 1991.

[7] H. Xie, *Fractals in Rock Mechanics*, A A Balkema Publishers, Avereest, Netherlands, 1993.

[8] H. Nagahama, "Fracturing in the solid earth," *Translated World Seismology*, vol. 61, no. 2, pp. 103–126, 1991.

[9] H. Xie, "Fractal nature on damage evolution of rock materials," in *International Symposium on Application of Computer Methods in Rock Mechnics and Engineering*, pp. 697–704, Xi'an, China, 1991.

[10] H. Xie, "The fractal effect of irregularity of crack branching on fracture toughness of brittle materials," *International Journal of Fracture*, vol. 41, no. 4, pp. 267–274, 1989.

[11] H. Xie, F. Gao, H. Zhou, and J. Zuo, "Fractal study on rock fracture and fragmentation," *Journal of Disaster Prevention and Mitigation Engineering*, no. 4, pp. 1–9, 2003.

[12] L. Shi, J. Xu, E. Bai, and Z. Gao, "Study on rock impact failure based on fractal theory," *Journal of Vibration and Shock*, vol. 32, no. 5, pp. 163–166, 2013.

[13] L. Shi, J. Xu, J. Liu et al., "Energy analysis of dynamic destruction process of sericite quartz and sandstone," *Chinese Journal of Underground Space and Engineering*, vol. 7, no. 6, pp. 1181–1185, 2011.

[14] J. Xu and L. Shi, "Analysis of energy consumption law of rock deformation and failure process under high temperature in SHPB test," *Chinese Journal of Rock Mechanics and Engineering*, vol. 32, no. 2, pp. 3109–3115, 2013.

[15] J. Xu and L. Shi, "Fractal characteristics analysis of marble impact loading test fragments," *Rock and Soil Mechanics*, vol. 33, no. 11, pp. 3225–3229, 2012.